Supporting information for

Fluorination of anatase TiO_2 towards titanium oxyfluoride $TiOF_2$: novel synthesis approach and proof of Li-insertion mechanism.

Nicolas Louvain,[1,2]*† Zouina Karkar,[1,2] Malika El-Ghozzi,[1,2] Pierre Bonnet,[1,2] Katia Guérin,[1,2] Patrick Willmann[3]

[1]Clermont Université, Université Blaise Pascal, Institut de Chimie de Clermont-Ferrand, BP 10448, F-63000 Clermont-Ferrand, France; [2]CNRS, UMR 6296, Institut de Chimie de Clermont-Ferrand, F-63177 Aubière, France; [3]Centre National d'Etudes Spatiales, Toulouse, France

Corresponding Author

E-mail address: nicolas.louvain@um2.fr. Telephone: +33 4 67 14 33 09. Fax: +33 4 67 14 33 04.

Present Address

†Institut Charles Gerhardt UMR CNRS 5253 (AIME), Université Montpellier 2, CC1502, place E. Bataillon, 34095 Montpellier cedex 5, France.

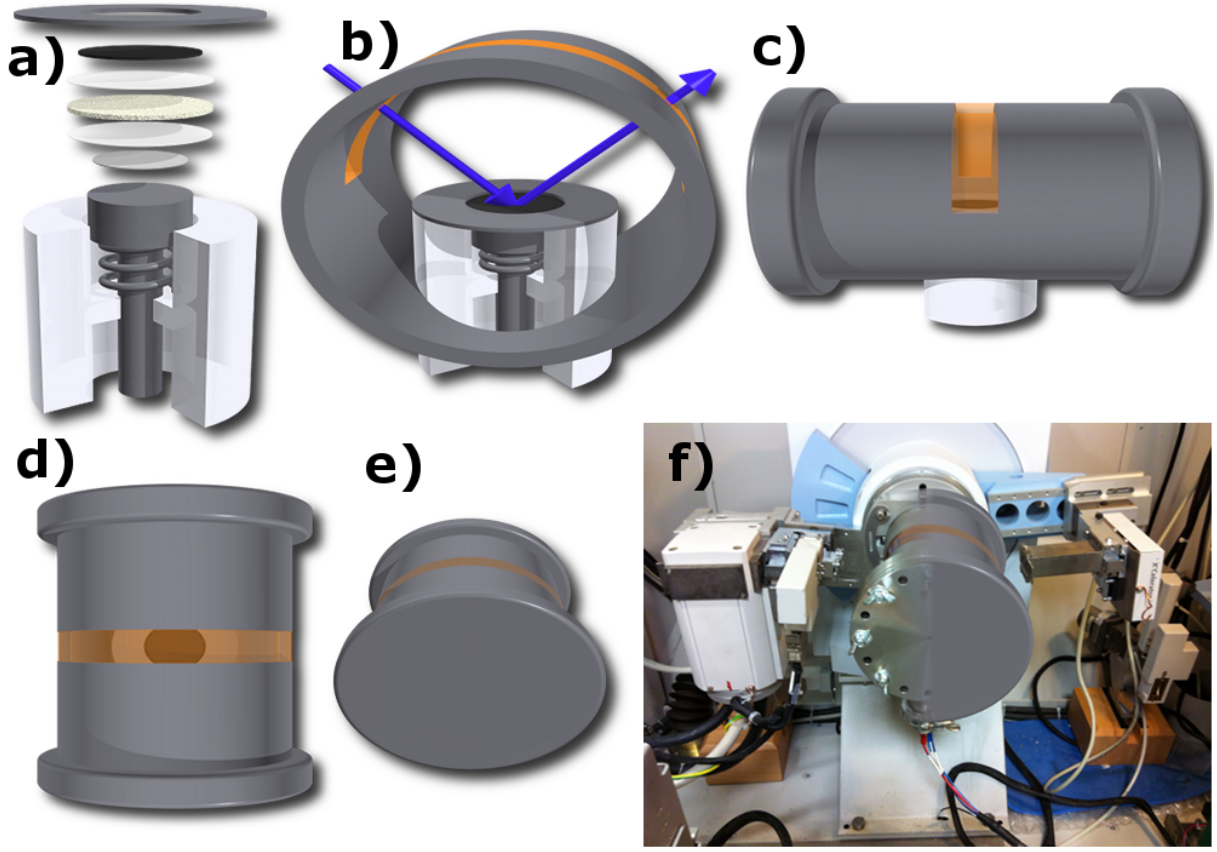

Figure S1. Schematic representation of *in situ* XRD environment-controlled cell (pressurized with argon) showing its core and parts (a), the mounted core inside its metallic alloy body (open here for display purposes but the only aperture through the body is at its bottom, where the core is inserted) and the kapton window allowing the X-ray (blue arrows) through (b), and the complete mounted cell viewed from the side (c), top (d) and front (e); the schematic model of the *in situ* cell is displayed over the real experimental model of the cell, shown installed on the X'Pert diffractometer (f); the connection between the cell and PC can be seen at the bottom at the image.

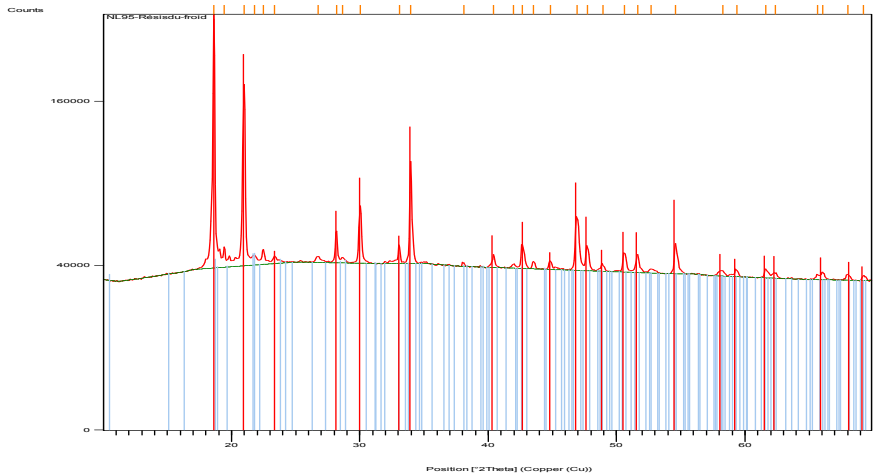

Figure S2. Indexing of XRD pattern of a crystalline residue obtained at the end of the fluorination of rutile TiO_2 (the red lines indicate theoretical peak positions of nickel titanium fluoride hydrate $NiTiF_6$; H_2O, PDF #00-025-0588)

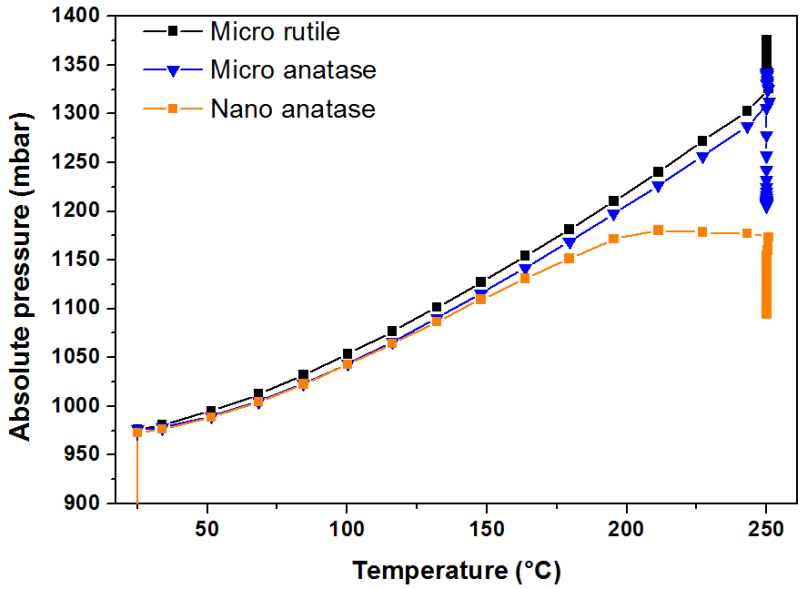

Figure S3. Evolution of the absolute pressure versus temperature of rutile and anatase powders under a mixture of N_2/F_2 gases during the heating process towards 250 °C.

Table S1. Size calculation results obtained from XRD peaks full-width at half minimum (FWHM) for different powders of TiO_2 and $TiOF_2$ (instrumental width was estimated with single crystalline Si film).

	FWHM (°)	Beta (°)	2-Theta (°)	Size (nm)	Size (µm)
TiO_2 anatase nano	0.43979	0.29591	25.35297	27.5	0.0275
TiO_2 anatase micro	0.19434	0.05046	25.35297	>150.0	>0.1500
TiO_2 rutile micro	0.14602	0.00214	27.44187	>150.0	>0.1500
Anatase-derived $TiOF_2$	0.39334	0.24946	23.43117	32.5	0.0325

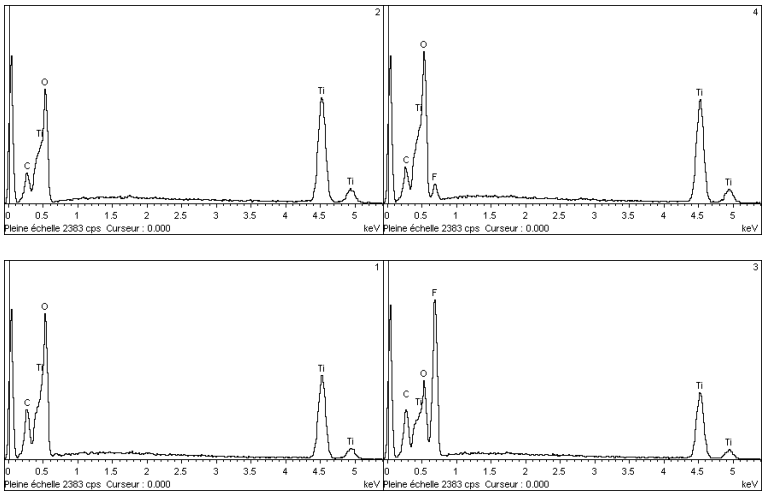

Figure S4. SEM images and EDX analyses of pristine (top left) and fluorinated (top right) rutile TiO_2; SEM images and EDX analyses of pristine (bottom left) and fluorinated (bottom right) anatase TiO_2.

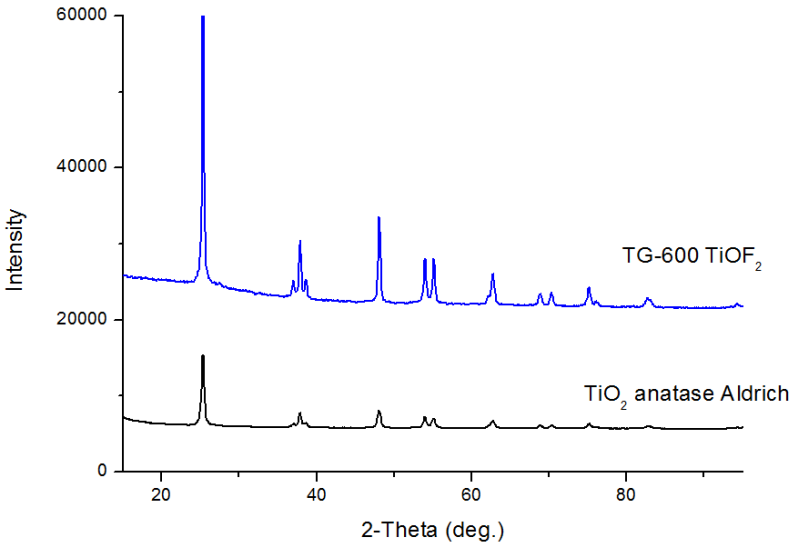

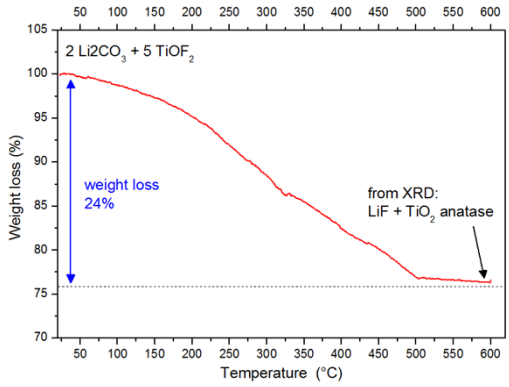

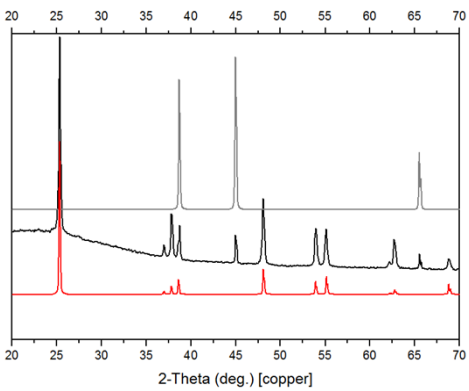

Figure S5. XRD of $TiOF_2$ after TG analysis up to 600 °C, compared with that of pristine TiO_2 powder (top); TG analysis of a stoichiometric mixture of Li_2CO_3 and $TiOF_2$ (bottom left) and the corresponding XRD pattern after TG analysis (bottom right); the XRD pattern is compared to simulated patterns of LiF (grey) and anatase TiO_2 (red).

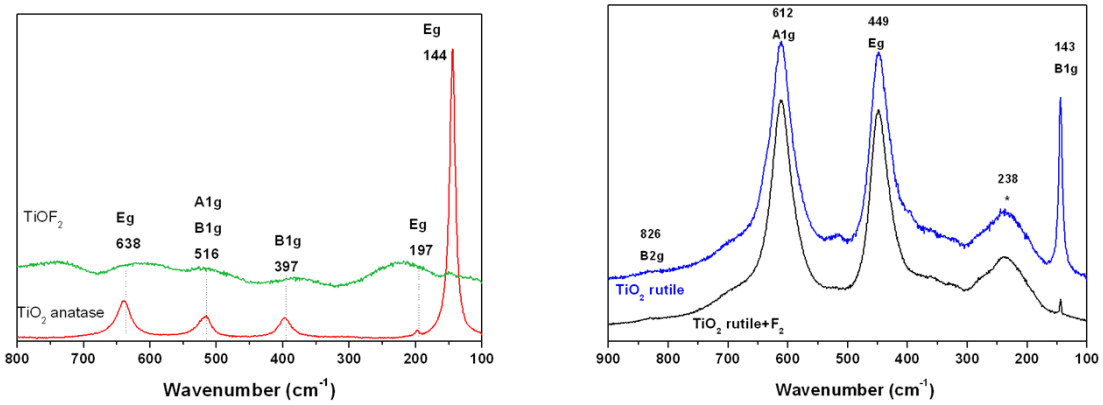

Figure S6. Raman spectra of anatase TiO_2 and anatase-derived $TiOF_2$ powders (left) and of rutile TiO_2 and rutile-derived fluorinated TiO_2 powders (right)

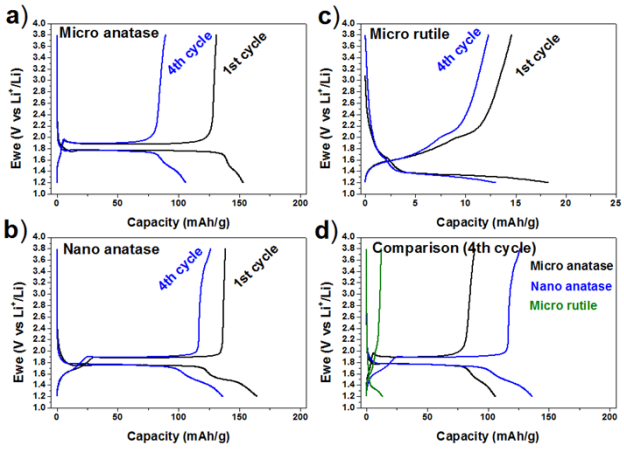

Figure S7. Galvanostatic charge-discharge profiles for different Li/TiO_2 cells cycled at C/20 between 3.8 and 1.2 V

Table S2. Main electrochemical results of different Li/TiO_2 cells cycled at C/20 between 3.8 and 1.2 V

Compound	Cycle	E_{oc}	Q_{red}	$E_{1/2}$(red)	Q_{ox}	$E_{1/2}$(ox)	C.E.
Micro anatase (a)	1st	3.138 V	154 mAh g^{-1}	1.766 V	132 mAh g^{-1}	1.875 V	85.7%
	4th	-	106 mAh g^{-1}	1.757 V	90 mAh g^{-1}	1.893 V	84.9%
Micro rutile (c)	1st	3.087 V	18 mAh g^{-1}	1.331 V	15 mAh g^{-1}	1.853 V	83.3%
	4th	-	13 mAh g^{-1}	1.328 V	12 mAh g^{-1}	1.827 V	92.3%
Nano anatase (b)	1st	3.159 V	165 mAh g^{-1}	1.745 V	139 mAh g^{-1}	1.876 V	84.2%
	4th	-	136 mAh g^{-1}	1.745 V	127 mAh g^{-1}	1.887 V	93.4%

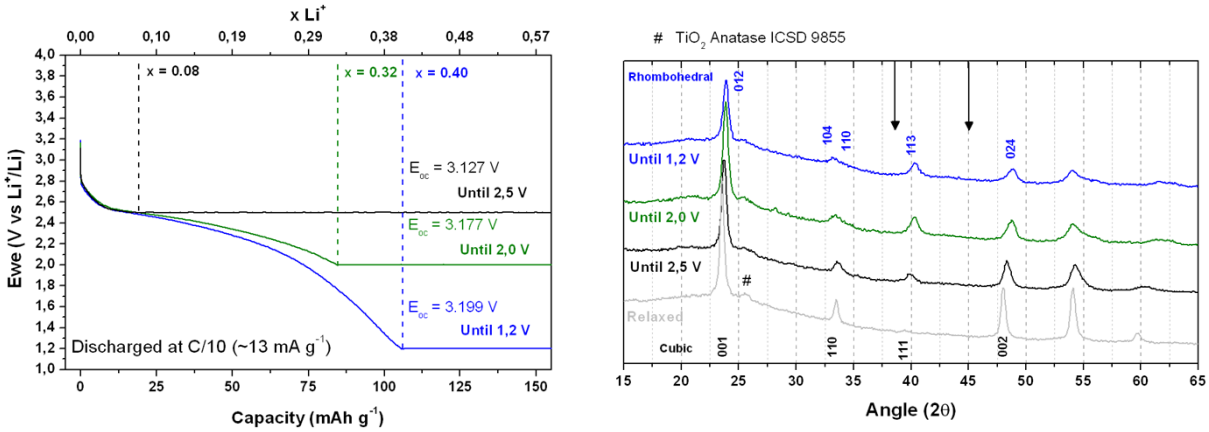

Figure S8. Galvanostatic discharge (at C/10) curves of three Swagelok-type cells of nanocrystals of $TiOF_2$ powders stopped at 2.5, 2.0 and 1.2 V (left) and their corresponding XRD patterns (right); the relaxed curve (i.e. not discharged) is shown for comparison. Miller indices for cubic (black) and rhombohedral (blue) $TiOF_2$ cells are noted, and the black downward arrows indicate the theoretical peak positions of LiF that are clearly absent from these four patterns.

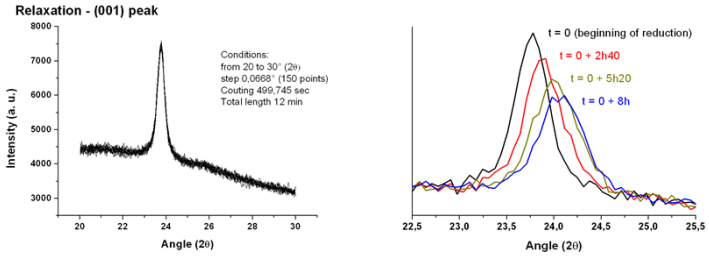

Figure S9. XRD patterns, showing the (001) peak of the cubic $TiOF_2$ phase, collected during the relaxation (left) and the first discharge (right) of the *in operando* XRD/electrochemistry measurement.

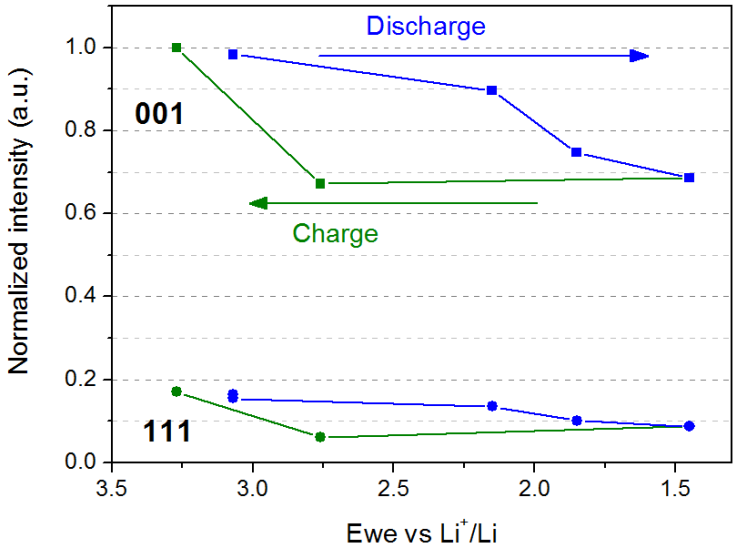

Figure S10. Evolution of the normalized intensities of the (001) and (111) peaks of the $TiOF_2$ phase during the *in operando* XRD/electrochemistry measurement of the first charge-discharge cycle.

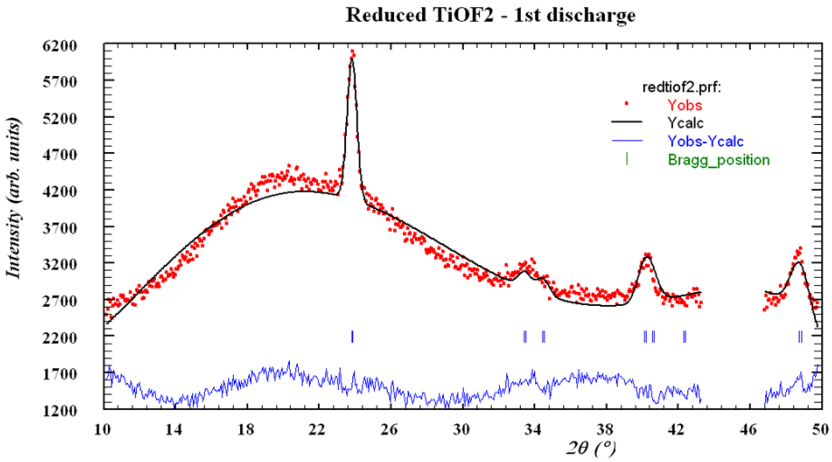

Figure S11. Profile matching refinement, using rhombohedral symmetry (*R*-3*c*), of the electrochemically lithiated $TiOF_2$ phase obtained at the end of the first discharge (at E = 1.2 V) during the *in operando* XRD/electrochemistry measurement. The peaks coming from the sample holder (made of an iron-nickel alloy) were removed from the refinement (42.5-47°).

Table S3. Profile matching results - Fullprof suite

```
-----------------------------------------------------------------------------------------------
-----------------------------------------------------------------------------------------------
No. H   K   L  Mult     Hw         2theta      Icalc       Iobs      Sigma    d-hkl
1   0   1   2     6  0.632534      23.803      873.6     1207.6    462.637    3.735026
2   1   0   4     6  0.844411      33.401      136.2       24.5     26.797    2.680492
3   1   1   0     6  0.867416      34.421      137.9      125.7     17.373    2.603324
4   1   1   3    12  0.997847      40.108      355.4      492.4    190.420    2.246350
5   0   0   6     2  1.008421      40.561      146.8      114.8     26.320    2.222292
6   2   0   2     6  1.048851      42.282        0.0        0.0      0.040    2.135729
7   0   2   4     6  1.204276      48.719      582.7      557.5     28.924    1.867513
-----------------------------------------------------------------------------------------------
BRAGG R-Factors and weight fractions for Pattern #  1
-----------------------------------------------------------------------------------------------
=> Phase:  1     Reduced TiOF2
=> Bragg R-factor:   25.1       Vol:  313.018( 0.636)  Fract(%):    0.00( 0.00)
=> Rf-factor=  15.2             ATZ:           0.000   Brindley:  1.0000
-----------------------------------------------------------------------------------------------
SYMBOLIC NAMES AND FINAL VALUES AND SIGMA OF REFINED PARAMETERS:
-----------------------------------------------------------------------------------------------
->  Parameter number    1 :           Bck_0_pat1     2640.8350    ( +/-     14.674967     )
->  Parameter number    2 :           Bck_1_pat1     1254.4122    ( +/-     156.83017     )
->  Parameter number    3 :           Bck_2_pat1     12646.334    ( +/-     486.01379     )
->  Parameter number    4 :           Bck_3_pat1    -48616.922    ( +/-     3064.5144     )
->  Parameter number    5 :           Bck_4_pat1    -170300.03    ( +/-     8907.5254     )
->  Parameter number    6 :           Bck_5_pat1    -113095.80    ( +/-     6845.3501     )
->  Parameter number    7 :       Scale_ph1_pat1    0.97557384    ( +/-    0.82320996E-01 )
->  Parameter number    8 :      Cell_A_ph1_pat1     5.2064366    ( +/-    0.53666928E-02 )
->  Parameter number    9 :      U-Cagl_ph1_pat1     5.4337010    ( +/-     2.9167769     )
->  Parameter number   10 :      V-Cagl_ph1_pat1    0.70955831    ( +/-    0.71708304     )
->  Parameter number   11 :      Cell_C_ph1_pat1     13.333917    ( +/-    0.18860878E-01 )
->  Parameter number   12 :           SyCos_pat1    0.24469224    ( +/-    0.42321835E-01 )
->  Parameter number   13 :       Bover_ph1_pat1    -10.000009    ( +/-     1.3600371     )

-----------------------------------------------------------------------------------------------
-----------------------------------------------------------------------------------------------
```